Journal of Physics: Conference Series

OPEN ACCESS

Advances in large-eddy simulation of a wind turbine wake

To cite this article: A Jimenez *et al* 2007 *J. Phys.: Conf. Ser.* **75** 012041

View the article online for updates and enhancements.

Journal of Physics: Conference Series **75** (2007) 012041 doi:10.1088/1742-6596/75/1/012041

Advances in large-eddy simulation of a wind turbine wake

A Jimenez[1,2], A Crespo[1] E Migoya[1]and J Garcia[1]

[1]Departamento de Ingeniería Energética y Fluidomecánica, ETSII, Universidad Politécnica de Madrid. C/José Gutiérrez Abascal, 2, CP.: 28006, Madrid, Spain.

[2]Corresponding author. Email to: a.jimenez@upm.es

Abstract. A CFD code has been developed based on a Large-Eddy Simulation (LES) approach. The turbine is simulated by concentrated drag forces, and is placed in an environment with turbulence anisotropy properties similar to the ones of the real atmosphere. Comparisons with experimental data and with analytical correlations have been performed, and the results are found to be in good agreement with both, suggesting that LES is a potentially useful tool in the investigation of detailed wake flow.

1. Introduction

Turbulence may be significantly large in wind turbine wakes, especially if turbines are clustered in arrays in which significant interference effects take place. The increase of turbulence intensity has to be taken into account adequately since important damage due to fatigue and dynamic loads occurs to downstream wind turbines, see Frandsen and Thögersen [1]. In this work we will show that a Large-Eddy Simulation (LES) approach is appropriate for studying the turbulence evolution in a wind turbine wake.

Different approaches, reviewed by Crespo *et al.* [2] and Vermeer *et al.* [3], have been adopted to study wind turbine wakes. The work presented here is a continuation of the UPMWAKE model proposed by Crespo *et al.* [4] and Crespo and Hernández [5], based on the *k-ε* closure methods, and the explicit algebraic model for the components of the turbulent stress tensor proposed by Gómez-Elvira *et al.* [6]. In all these methods, the Reynolds average over all turbulence scales was used. LES will reproduce the unsteady oscillations of the flow characteristics over all scales larger than the grid size; consequently, a greater detail of the turbulence characteristics is expected to be obtained. A LES model with simplified boundary conditions has been implemented in a CFD code to simulate and characterize the turbulence generated by the presence of a wind turbine. In this work we have performed the LES calculation of the wake placing the simplified turbine immersed in an environment with turbulence properties similar to the ones of the atmosphere. The wind turbine is modelled by drag forces applied at the grid points corresponding to the projected disk area. We present the results obtained by this new approach as well as a comparison with experimental data obtained by Cleijne [7] from the Sexbierum wind farm and with analytical correlations previously proposed by Crespo and Hernández [8] and Gomez-Elvira *et al.* [6]. In future work, other possibilities of LES technique that cannot be treated with the Reynolds averaged Navier Stokes equations will be explored. In particular, the meandering effect in the wake, caused by oscillation in the direction of wind speed, is an important topic of study. Other points of interest that a LES simulation would allow to investigate are the spectral analysis and the spatial coherence of turbulence variables of the wake.

2. Governing equations

We consider a three-dimensional airflow of incompressible and viscous fluid moving between two parallel planes (channel flow). In a LES simulation, the flow variables are divided into a grid-scale (GS) part and a subgrid-scale (SGS) part by the filtering operation. The effect of the unresolved SGSs is parameterized by the eddy viscosity assumption of Smagorinsky [9], through the following constitutive relations:

$$\tau_{ij}^{(SGS)} = \frac{\tau_{kk}^{(SGS)}}{3}\delta_{ij} - 2\rho\nu_T \overline{S}_{ij} \tag{1}$$

$$\nu_T = C_S^2 \Delta^2 \left\| \overline{\mathbf{S}} \right\| \tag{2}$$

$$\left\| \overline{\mathbf{S}} \right\| = \left(2\overline{S}_{ij} \cdot \overline{S}_{ij} \right)^{\frac{1}{2}} \tag{3}$$

$$\overline{S}_{ij} = \frac{1}{2}\left(\frac{\partial \overline{u}_i}{\partial x_j} + \frac{\partial \overline{u}_i}{\partial x_i} \right) \tag{4}$$

$$\Delta = \left(\Delta_x \Delta_y \Delta_z \right)^{\frac{1}{3}} \tag{5}$$

where δ_{ij} is the Kronecker delta, ν_T is the eddy viscosity, $\overline{S}_{ij}$ is the resolved strain rate tensor, $\left\| \overline{\mathbf{S}} \right\|$ is the magnitude of the resolved strain rate tensor, Δ is the grid-filter width, which is a characteristic length scale of the largest SGS eddies, and Δ_x, Δ_y and Δ_z are the grid spacings in the three axis directions. In the original Smagorinsky model (Smagorinsky [9] and Lilly [10]) the dimensionless parameter C_S is an empirical constant of value $0{,}1 \sim 0{,}18$ whereas in the dynamic Smagorinsky model (Germano *et al.* [11]) this parameter is computed dynamically during the solution making it a function of space and time. The dynamic model is adopted in this work.

Finally, defining a *pseudopressure* in the following way:

$$p^* = \overline{p} + \frac{\tau_{kk}^{(SGS)}}{3} \tag{6}$$

the governing equations present the form:

$$\frac{\partial \overline{u}_i}{\partial x_i} = 0 \tag{7}$$

$$\frac{\partial \overline{u}_i}{\partial t} + \frac{\partial \overline{u}_i \cdot \overline{u}_i}{\partial x_j} = -\frac{1}{\rho}\frac{\partial p^*}{\partial x_i} + \frac{\partial}{\partial x_j}\left[2\left(\nu + \nu_T \right) \overline{S}_{ij} \right] \tag{8}$$

Temporal averages will be indicated by a bracket, $\langle \cdot \rangle$, and their fluctuations, that is the instantaneous filtered value of a flow magnitude minus its time average value, are indicated by an apostrophe, ': $\overline{\phi} = \langle \overline{\phi} \rangle + \overline{\phi}'$, where ϕ is any of the flow variables, velocity or pressure. As the average process is steady, time averages will also be the classical Reynolds average. In the following we will always operate with filtered values and for simplicity we will omit the bar. The subgrid-scale (SGS) stresses (see equation (1)) are found to be negligible compared with the resolved ones, $\left| \langle \tau_{ij}^{(SGS)} \rangle \right| < 0.01 \left| \rho \langle u'_i u'_j \rangle \right|$. Thus, it is justified to assume that most of the energy and momentum transport rate are contained in the resolved fluctuations; therefore only the filtered values are considered in the following discussion.

3. Numerical scheme

A set of channel flow simulations have been performed using the code elaborated at Center for Turbulence Research, Stanford University by Charles D. Pierce (see Pierce and Moin [12], and Wall *et al.* [13]). The numerical method used to solve the equations (7) and (8) is a semi-implicit iterative solution procedure that is both economical but also retains most of the stability and accuracy properties of the fully implicit scheme. It is conveniently described in those references. The calculations have been performed with a grid of 256 × 96 × 96 points in *x*, *y* and *z* directions respectively, which, considering the size of the computational domain described below ensures a good quality in the shape of the cells. In the vertical direction, the grid points are non-uniformly distributed, particularly they have been clustered around the turbine. The first grid point is placed at a distance of 0,036*h* over the ground, where *h* is the wind turbine hub height. Grid convergence has been verified~~,~~ by checking that time average results do not change significantly with an increase of the number of grid points.

4. Flow model

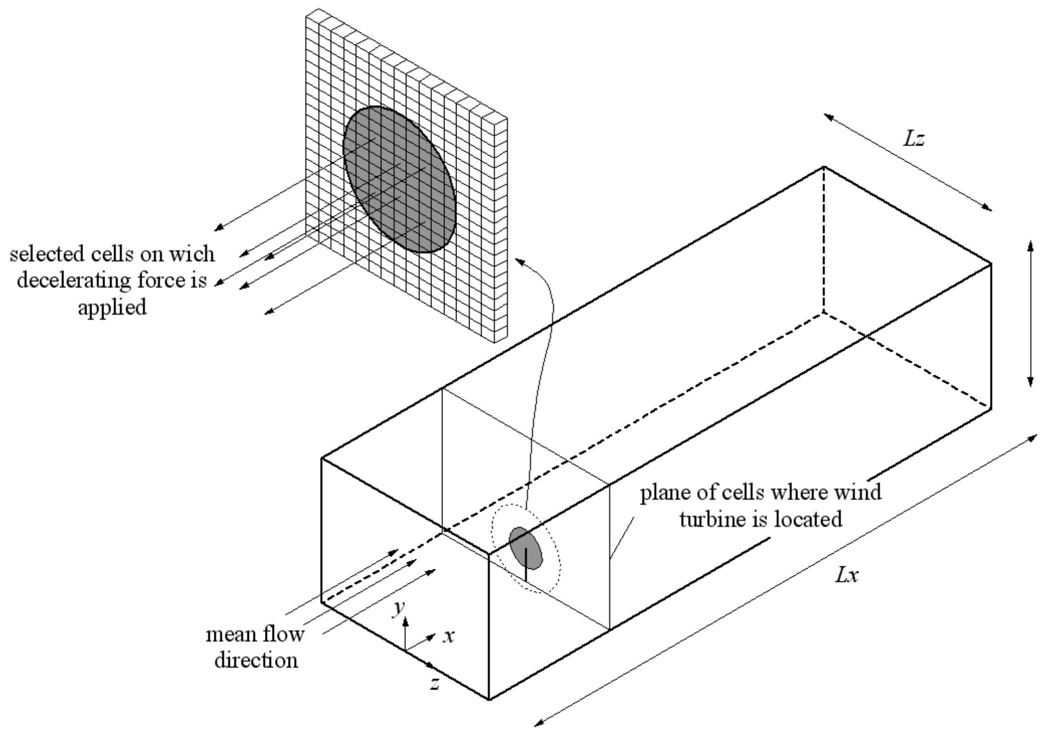

Figure 1. Schematic view of the computational domain.

The configuration to be studied is shown in Figure 1. The computational domain is a rectangular channel of the shape of a parallelepiped whose sides have lengths L_x=34,9*D*, L_y=5,6*D*, and L_z=10,7*D*, where *D* is the wind turbine diameter. Inside the box there is the wind turbine, which is simulated by several momentum sinks. On the side walls of the channel, $z=\pm L_z/2$, periodic boundary conditions are applied. For the upper wall, a boundary condition giving a fix value of the shear stress is imposed. Periodic boundary conditions are also applied at the entrance plane, *x*=0, and the exit $x=L_x$. Thus, the flow field that is represented corresponds to an infinite line of wind turbines separated the distance L_x. The length L_x is large enough so that the flow field incident over the wind turbine approximately corresponds to an unperturbed incident wind flowing over a single turbine. It is expected that this incident flow field will have the characteristics of a real atmospheric flow. In particular, that the average flow velocity in the *x* direction will be given by the classical law of the wall, which in the case of rough wall is expressed as:

$$\langle u_x \rangle = \frac{u^*}{\kappa} \ln \frac{y}{y_0} \tag{9}$$

where u^* is the friction velocity, κ is the von Karman constant (κ=0.4) and y_0 represents the terrain roughness. We will check later whether this law of the wall is really satisfied.

4.1. Wind turbine model

The next step is to introduce inside the airflow a model of wind turbine that allow us to understand how the presence of the turbine creates a wake and modifies the flow characteristics. The circular disk is approximated by a set of rectangular cells in a Cartesian grid. The model consists of the disk formed by the set of cells (see Figure 1) in which we introduce a force in the *x* direction, proportional to the area of each cell and to the square of the incident average velocity in the central cell:

$$f_x = -C_T \cdot \tfrac{1}{2} A u_0^2 \tag{10}$$

C_T represents the thrust coefficient of the wind turbine, A is the frontal area of the cell, and u_0 is the unperturbed velocity of the incident flow in the centre of the disk. The minus sign means that the force has opposite direction to that of the mean flow, and therefore, decelerates the incident stream. Such a model of wind turbine is like a porous disk, which occasionally has been used to simulate wind turbines. Larsen *et al.* [14] present results from 3D CFD computations, indicating that the near wake field may be separated in 2 regions, according to whether or not the flow structures around the turbine blades have developed to an azimuth invariant stage. The extend of the inner region (in which blade flow structures can be identified) is only of the order one rotor diameter. The tower shadow could also be simulated with a distribution of sinks; however as the frontal area of the tower is much smaller than that of the disk, and the expected drag coefficients of tower and disk are quite similar, the tower effect has been neglected. Nevertheless, some authors have commented on the relevance of the tower effect (Helmis *et al.* [15]), and in future works this will be considered. In the present study, the real blades of the turbine are not taken into account because we are not really interested in the local properties of the flow directly interacting with wind turbine blades, but in the downstream evolution of the flow characteristics. In particular, we principally want to study the turbulence added in the wake. That turbulence is mainly generated in the shear layer of the near wake. There is a core region where the flow is decelerated by the wind turbine, and outside it the velocity has the ambient value; the difference between these two velocities creates the shear layer that has a ring-like shape. Turbulent diffusion makes the shear layer thickness increase with downstream distance, and, at a certain distance downstream (about two to five diameters), the shear layer reaches the wake axis. It should be taken into account that this shear layer in the near wake is made up of concentrated vortices, and that the flow is not really turbulent outside them. The superficial resemblance to classical turbulent shear layers, as in wakes and mixing layers, occurs largely because wind turbine wakes are mostly viewed in an average sense: the flow at any point is treated as an ensemble average over many blade revolutions, so that azimuthal variations in the mean velocities, as seen by an observer rotating with the blades, appear as ‘‘turbulence’’ to a non-rotating observer.

4.2. Boundary conditions

The boundary condition in the bottom side of the computational domain, *y*=0, (see Figure 1) is expressed by the following equations, frequently used in meteorology:

$$u_y = 0 \tag{11}$$

$$\rho(\nu + \nu_T) \frac{\partial u_i(x,y,z)}{\partial y} = \tau_{iy}(x,z) \qquad i = x,z \tag{12}$$

where:

$$\tau_{iy}\left(x,z\right)=\rho\frac{\kappa^2}{\left[\ln\left(\frac{d}{y_0}\right)\right]^2}\left|u_h\left(x,z\right)\right|u_i\left(x,d,z\right)\qquad i=x,z \tag{13}$$

and

$$u_h\left(x,z\right)=\sqrt{u_x\left(x,d,z\right)^2+u_z\left(x,d,z\right)^2} \tag{14}$$

are proposed by Senocak *et al.* [16]. Very similar approaches are used by Moeng [17] and by Piomelli and Balaras [18]. In expression (12) τ_{iy} are the instantaneous global shear stresses at ground and d is the distance of the first node to the wall. Note that condition (13) is consistent with the law of the wall, equation (9), although in that equation the temporal average values of velocity and shear stress were used, whereas in the previous condition we are operating with instantaneous values; in particular:

$$\left\langle\tau_{xy}\left(x,y\right)\right\rangle=\rho u^{*2} \tag{15}$$

is the classical definition of u^* in the law of the wall.

In the top side of the domain, $y=L_y$, we adopt:

$$u_y=0 \tag{16}$$

$$\rho\left(\nu+\nu_T\right)\frac{\partial u_x}{\partial y}=\left\langle\tau_{xy}\left(x,z\right)\right\rangle=\rho u^{*2} \tag{17}$$

$$\frac{\partial u_z}{\partial y}=0 \tag{18}$$

Equation (17) guarantees a uniform value (that means no y-variation) of the average shear stress in the regions that are not affected by the wake.

5. Results and comparison with experiments

Comparison has been made with the experimental results obtained by Cleijne [7] in the Sexbierum wind farm. This wind farm is in the North of the Netherlands, and has 18 turbines of 300 kW of rated power, a diameter of D=30 m and a hub height of h=35 m. In this application only measurements corresponding to an isolated wind turbine are considered. At velocities in the range 7-10 m/s, the thrust coefficient of the turbine is C_T=0,75. The calculations presented have been performed with a wind velocity of u_0=10 m/s at hub height, and a surface roughness of y_0=0,05 m, giving u^*=0,61 m/s. For comparison with the numerical calculations the results are presented in non-dimensional form. Because of the large spatial scales, it is expected that the Reynolds number effects be not important, and that the air molecular viscosity will be negligible compared to the turbulent eddy viscosity.

5.1. Comparison of the characteristics of the incident flow over the turbine with those of the atmospheric flow

In Figure 2a is given the calculated velocity profile incident over the turbine and is compared with the logarithmic law expressed in equation (9); the agreement is good in the zone where the wind turbine is placed. In the upper part of the domain the calculated value of the velocity is larger than the one given by the law of the wall; this is due to the boundary conditions (16) to (18); in future works we will try to correct this effect. In Figure 2b, are shown the distributions of all the calculated components of the Reynolds stress tensor $\left\langle\tau_{ij}\right\rangle=-\rho\left\langle u_i'u_j'\right\rangle$. The SGS stresses $\tau_{ij}^{(SGS)}$ are found to be completely negligible compared with the resolved ones, except for the component τ_{xy} in a very small region close to the walls, since at them u_y=0 at any time, and then u'_y=0. The components $\left\langle\tau_{xz}\right\rangle$ and $\left\langle\tau_{yz}\right\rangle$ are zero because of symmetry. As indicated in equation (15), the mean turbulent shear stress of the incident flow should be $\left\langle\tau_{xy}\right\rangle=\rho u^{*2}$ which is in excellent agreement with the calculated value. The numerically predicted values of the three diagonal components are not too far from those measured in the Sexbierum wind farm, as can be seen in Figure 2b.

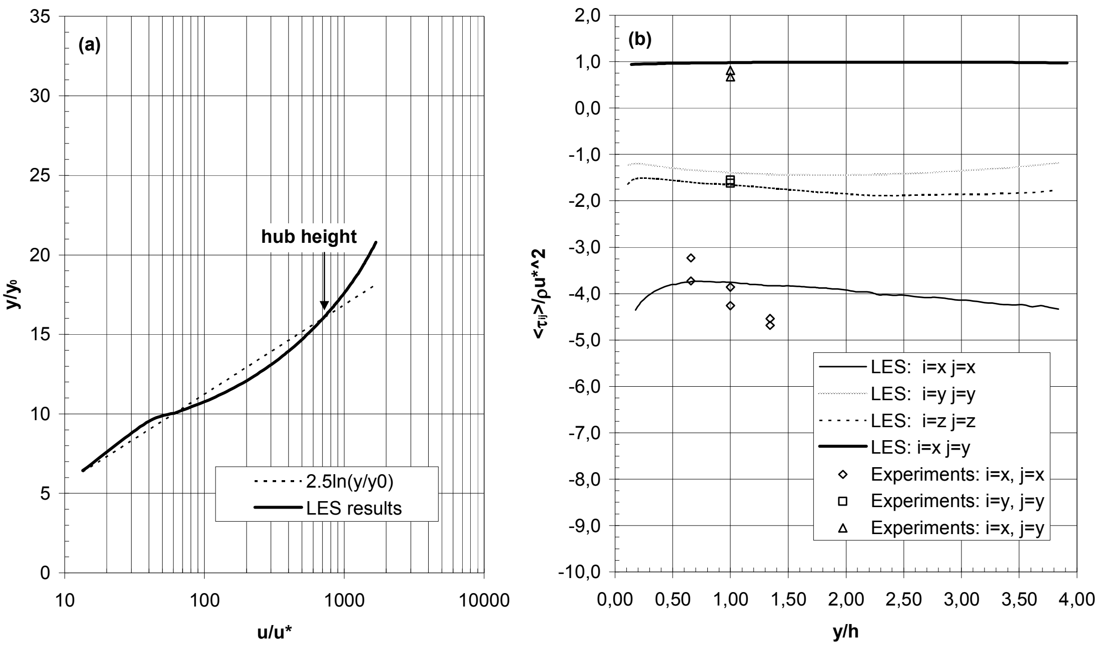

Figure 2. Incident flow over the turbine. (a) Velocity profile and law of the wall. (b) Reynolds stress components profiles compared with those measured at Sexbierum wind farm.

5.3. *Comparison of wake results*

In Figures 3 to 6 we present the results obtained by the LES calculation and its comparison with the available experimental data, related to Reynolds stress tensor components. The angle represented in horizontal coordinate axis corresponds to the angle between wind direction and the direction joining the sensor and the turbine (for instance, the angle 0º corresponds to the wind direction aligned with the direction joining the sensor and the turbine).

Figure 3 shows the values of the dimensionless turbulence fluctuations in the average flow direction, $\langle u_x'^2 \rangle^{\frac{1}{2}} / u_0$, and vertical direction, $\langle u_y'^2 \rangle^{\frac{1}{2}} / u_0$, in the near wake at hub height for different wind directions. The diagonal element of the turbulence stress tensor that is not represented, $\langle u_z'^2 \rangle^{\frac{1}{2}} / u_0$, has values in between the two others. There is a clear non-symmetric behaviour of the experimental results that obviously could not be reproduced with the model that has been used, and which may be due to the effect of other turbines or some obstacle. The code reproduces satisfactorily the measured value of the turbulence intensity in the flow direction in the peaks observed around 10º-20º. These peaks correspond to the shear layer that is formed in the near wake. These peaks are not observed for the vertical turbulence intensity, whose calculated values agree well with experimental results. Experiments show that at the wake centre $\langle u_x'^2 \rangle^{\frac{1}{2}} / u_0$ and $\langle u_y'^2 \rangle^{\frac{1}{2}} / u_0$ become equal, however, the calculations do not reproduce this behaviour and the calculated value of the turbulence intensity in the flow direction is slightly higher than the measured one. The reasons for this discrepancy are being studied. In the calculations carried out with the algebraic stress model by Gómez-Elvira *et al.* [6] this isotropic behaviour in the core of the near wake was better reproduced.

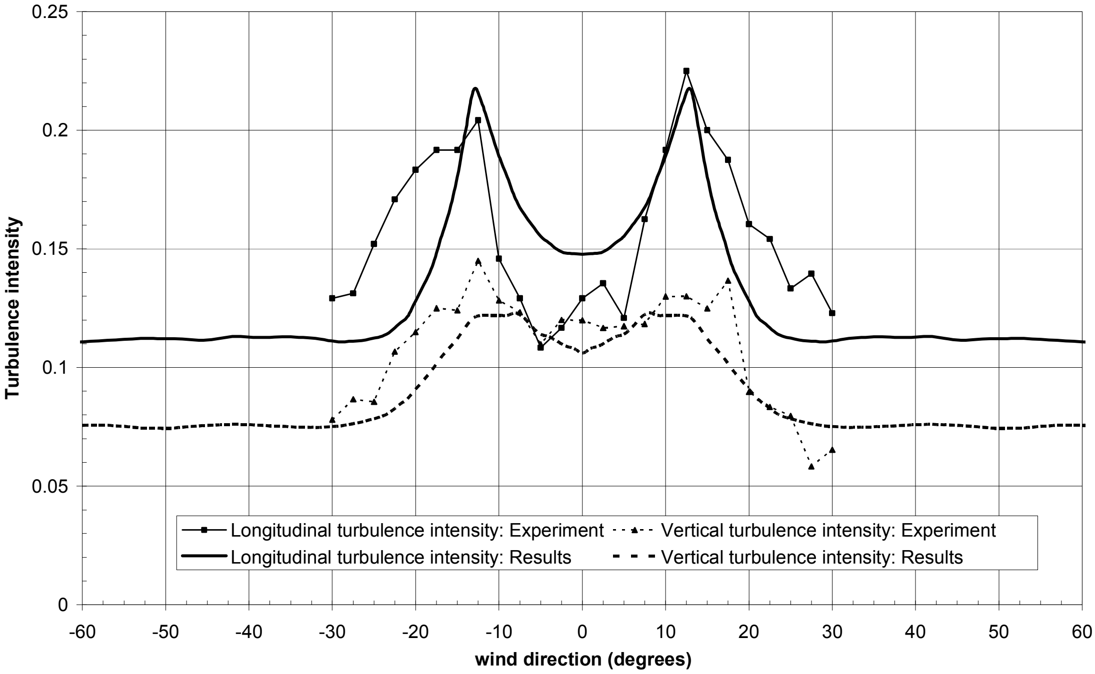

Figure 3. Turbulence intensity in the average flow direction, $(\langle u_x'^2\rangle)^{1/2}/u_0$ and vertical direction $(\langle u_y'^2\rangle)^{1/2}/u_0$, at a downstream distance of 2.5*D*, in a horizontal plane at hub height.

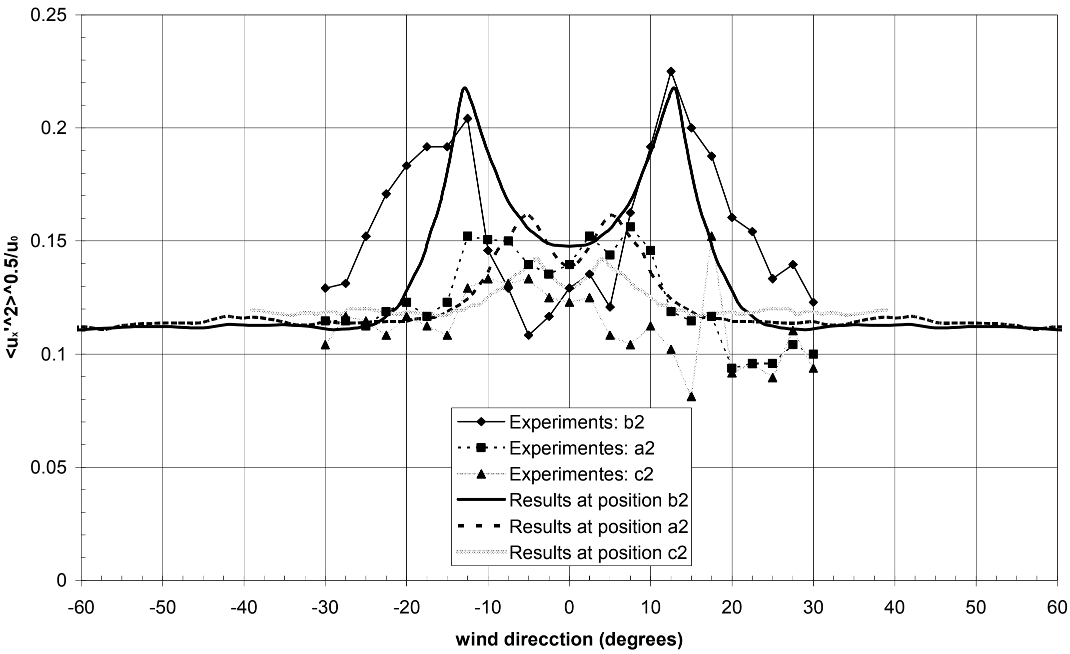

Figure 4. Turbulence intensity in the average flow direction, $(\langle u_x'^2\rangle)^{1/2}/u_0$, at several downstream distances of 2.5*D* (anemometer b2), 5.5*D* (anemometer a2) and 8*D* (anemometer(c2), in a horizontal plane at hub height.

We present in Figure 4 the evolution of the streamwise turbulence intensity as we move downstream, and it is compared with experimental data. We can observe again the non-symmetric values of turbulence intensity measurements; obviously, this behaviour can not be simulated with calculations. Agreement is better with the measurements on the right hand side. The turbulence created by the turbine at a downstream distance of 8 diameters is still important. The experimental results at that distance have an irregular and disordered behaviour.

Figure 5 shows the dimensionless distribution in a horizontal plane of correlation $\langle u_x 'u_z '\rangle / u_0^2$ at hub height. The agreement with experimental results is good. As expected, because of symmetry, $\langle u_x 'u_z '\rangle / u_0^2$ is equal to zero in the centre and in both sides outside the wake. There is a maximum in the shear layer, which is also in agreement with a gradient-type eddy viscosity model. This maximum is very large, about four times the value of the shear stress u^{*2}/u_0^2 in the unperturbed ambient flow. The position of the maximum is well predicted by our code, while the calculated value of the peak is somewhat smaller than the measured one. The correlation $\langle u_y 'u_z '\rangle / u_0^2$, which corresponds to the shear in a vertical plane perpendicular to the wind direction, is not presented; it has a similar behaviour as that of Figure 5, although with a smaller peak, and there are not measurements for it.

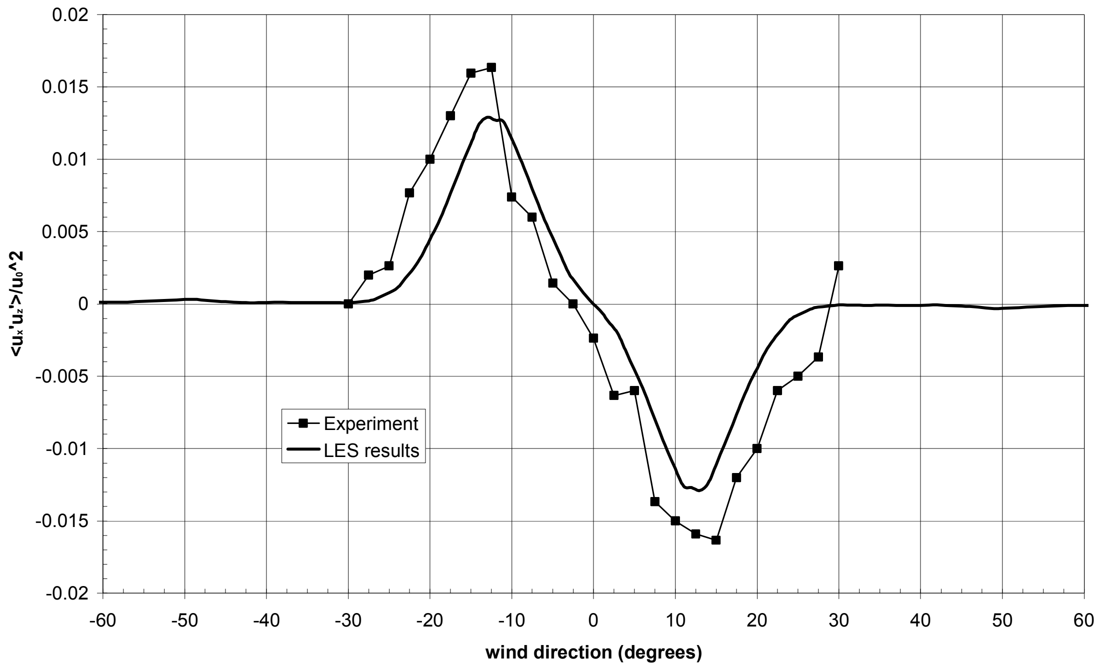

Figure 5. Non-dimensional correlation of fluctuating velocities $<u_x’u_z’>/u_0^2$, at a downstream distance of 2.5D, in a horizontal plane at hub height.

The results of the shear stress correlation $\langle u_x 'u_y '\rangle / u_0^2$ are presented in Figure 6. Two peaks located near the shear layer can be noted. In the core of the near wake there is a minimum of the shear stress. As it happens with the previous figure, this is expected, because the velocity is more uniform in the core than in the shear layer. This minimum did not appear in the calculations of Gómez-Elvira *et al*. [6], using an explicit algebraic stress model. Regarding the comparison with experiments, the qualitative shape of the profile is well estimated, although this comparison is not easy because of the asymmetries and the irregular behaviour of experimental data. Again, agreement seems to be better for data on the right hand side. In addition, we want to mention that a much more rapid decay with downstream distance has been observed for this correlation than for the diagonal components of the turbulence stress tensor.

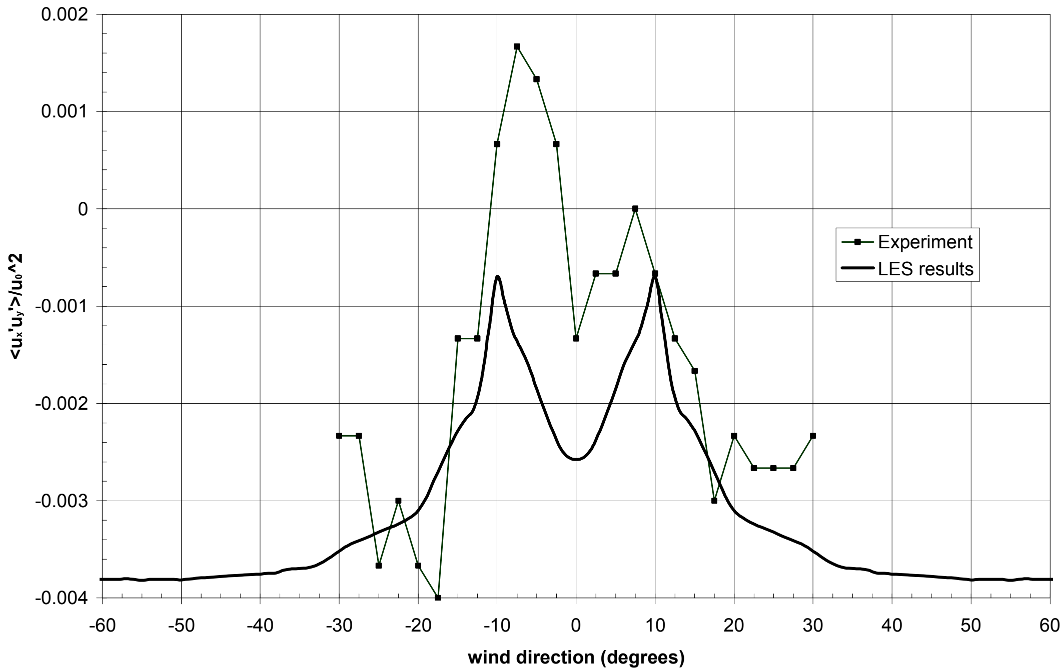

Figure 6. Non-dimensional correlation of fluctuating velocities $<u_x'u_y'>/u_0^2$, at a downstream distance of 2.5*D*, in a horizontal plane at hub height.

6. Analytical correlations

In addition to comparison with experimental data, it is interesting to review some correlations previously proposed, both in the near and far wake regions.

6.1. Near wake

Based on analytical solution of the Reynolds stress model, applicable in the shear layer of the near wake, where production dominates over dissipation, Gómez-Elvira *et al.* [6] propose the following expressions

$$\Delta I_{x,\max} = \frac{\sqrt{\Delta \langle u_x'^2 \rangle_m}}{u_0} = 0.447\left(1-\sqrt{1-C_T}\right) \tag{19}$$

$$\Delta I_{y,\max} = \frac{\sqrt{\Delta \langle u_y'^2 \rangle_m}}{u_0} = \Delta I_{z,\max} = \frac{\sqrt{\Delta \langle u_z'^2 \rangle_m}}{u_0} = 0.158\left(1-\sqrt{1-C_T}\right) \tag{20}$$

where C_T is the thrust coefficient. Crespo and Hernández [8] proposed an alternative expression based on an analytical solution of the *k*-*ε* model; then, the predicted $\Delta I_{x,\max}$ turns out to be smaller than that given by equation (19):

$$\Delta I_{x,\max} = 0.362\left(1-\sqrt{1-C_T}\right) \tag{21}$$

In Figure 7a, is given a comparison of these simple expressions (19) and (21) with some experimental results from Cleijne [7], Smith and Taylor [19], Talmon [20], Taylor [21], Hassan *et al.* [22], Högström *et al.* [23] and Højstrup [24], that has already been discussed in Gómez-Elvira *et al.* [6] and Crespo and Hernández [8].

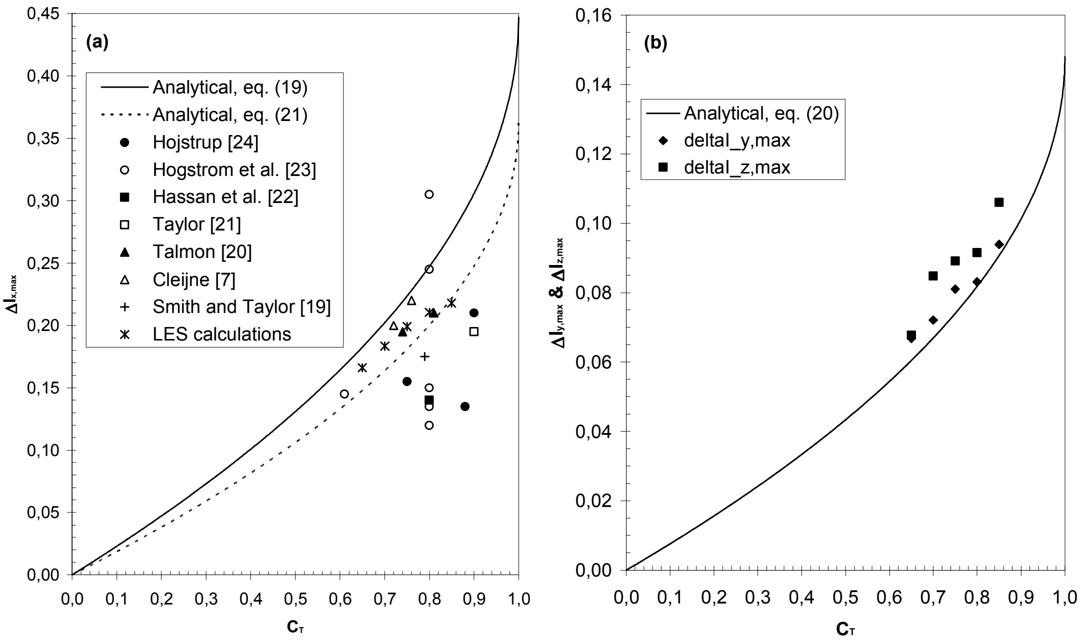

Figure 7. Maximum value of the added turbulence intensity: (a) streamwise direction; (b) spanwise and vertical directions (b).

In all cases, the maximum numerical value of $\Delta I_{x,\max}$ was obtained within a region from one to four rotor diameters downstream, and, as expected from previous considerations, occurred in the upper part of the wake. Our numerical results follow the tendencies of equations (19) and (21), being closer to the second one as thrust coefficient increases.

A comparison between the turbulence intensities in the spanwise and vertical directions predicted by eq. (20) and the results from our calculations is shown in Figure 7b. The agreement for the vertical turbulence intensity is quite good, better than the agreement with the calculated values of the turbulence intensity in the transverse horizontal direction.

6.2. Whole (near and far) wake

In Figure 8, taken from Frandsen [25], are shown the results of three correlations proposed by Quarton [26], Crespo and Hernández [8] and Frandsen and Thögersen [1], respectively, for the decay with downstream distance of the added turbulence intensity. Quarton's and Crespo and Hernández's correlations are expected to be valid only for the far wake. The results of that figure are supposed to correspond to hub height velocities in the range 9-11 m/s, which roughly correspond to a thrust coefficient of C_T=0,7. Frandsen`s correlation is being used in the recent version of the International Standard IEC 61400-1 Ed.3 [27]. Some experimental results presented in Frandsen [25] (Ghaie, personal communication, 1997) are also shown in Figure 8. In that figure we also represent the maximum values of the added turbulence across the wake*,* calculated with the LES procedure and the turbine configuration previously indicated, and with C_T=0,7. These results are in good agreement with Crespo and Hernández's correlation, and are slightly smaller than those given by Frandsen's correlation. They are also in good agreement with some of the experimental results. However, it is not clear whether all the experimental results correspond to C_T =0,7.

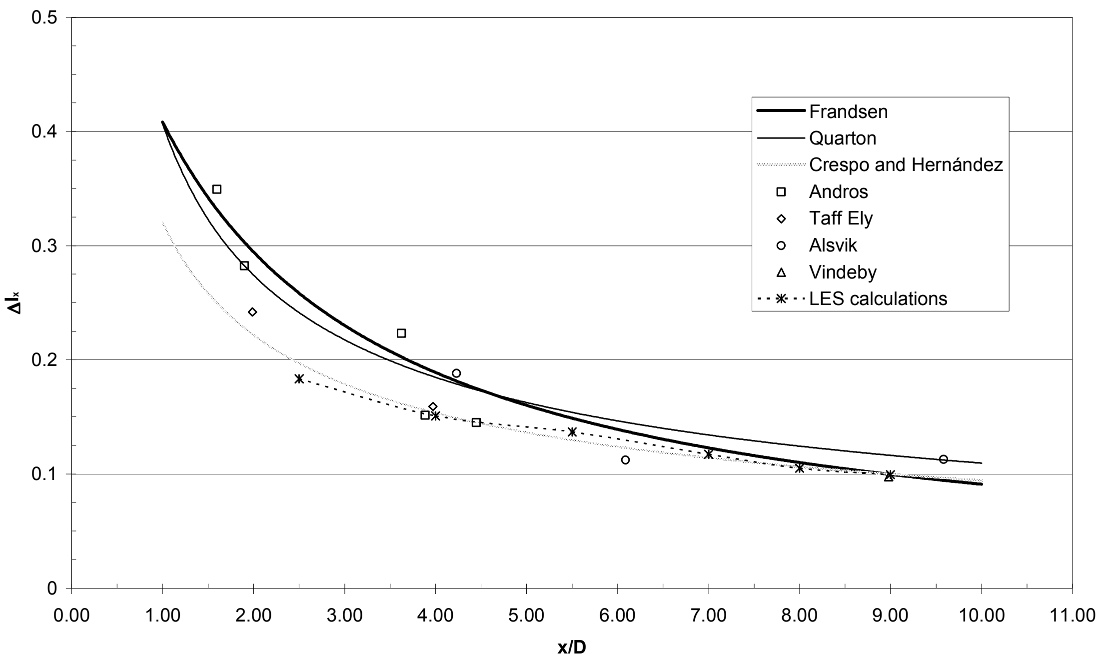

Figure 8. Correlations for the variation of the added turbulence intensity in streamwise direction in the wake. In the experiments considered the velocities are in the range 9 m/s < u_0 < 11 m/s. For the LES calculation a value of C_T=0,7 is assumed.

7. Conclusions and future work

A simplified LES model is proposed to simulate the turbulent flow in the wake of a wind turbine. The turbine is simulated by a set of local sinks of momentum distributed across the rotor disk, without reproducing the blade details. The turbulence characteristics, in particular the six components of the Reynolds stress tensor at every point of the computational domain have been obtained and found to be in good agreement with experimental results, with other calculations and with analytical correlations established in the literature. These results indicate that this LES model, with the simplified approach to simulate the rotor, is a very useful tool to simulate real turbulent characteristics in wakes. However, the method gives information not only on the average turbulence characteristics, but of the detailed flow oscillations and eddies in scales larger than the grid distance. Consequently other turbulence characteristics such as spectra, limit values of flow fluctuations, etc. can be reproduced with this model. This will be done in future work. Also, the meandering effect in the wake, caused by oscillations in the direction of incident wind speed, is an important topic of study that is specifically amenable to study with this model. For this study the spectra of the horizontal velocity component of the atmospheric flow that display spectral densities that are larger at low frequencies than those of vertical components will have to be reproduced. In Mann [28] and in the International Standard IEC 61400-1 Ed.3 [27], are given indications of how to reproduce the incident atmospheric flow. It is also well known that spatial coherence is an important characteristic of turbulence, related to fatigue loading in wind turbines, see Larsen and Hansen [29]; the method proposed in this paper could be a useful tool to study spatial coherence of turbulence, both in the incident and wake flows.

8. References

[1] Frandsen S and Thögersen M L 1999 Integrated fatigue loading for wind turbines in wind farms by combining ambient turbulence and wakes *Wind Eng.* **23 (6)** 327–340
[2] Crespo A, Hernández J and Frandsen S 1999 A survey of modelling methods for wind turbine wakes and wind farms. *Wind Energy* **2** 1-24

[3] Vermeer L J, Sørensen, J N and Crespo A 2003 Wind turbine wake aerodynamics. *Prog. Aero Space Sci* **6–7**, 467–510

[4] Crespo A, Manuel F, Moreno D, Fraga E and Hernández J 1985. Numerical analysis of wind turbine wakes *Bergeles G and Chadjivassiliadis J (Eds) Proceedings of the Delphi Workshop on Wind Energy Applications* 15-25

[5] Crespo A and Hernández J 1989 Numerical modelling of the flow field in a wind turbine wake. *Proceedings of the 3rd Joint ASCE/ASME Mechanics Conference Forum on Turbulent Flows ASME FED* **76** 121-127

[6] Gómez-Elvira R, Crespo A, Migoya E, Manuel F and Hernández J 2005. Anisotropy of turbulence in wind turbine wakes *J. Wind Eng. Ind. Aerodyn.* **93** 797-814

[7] Cleijne J W 1992 Results of Sexbierum Wind Farm Report *MT-TNO Apeldoorn* 92-388

[8] Crespo A and Hernández J 1996 Turbulence characteristics in wind turbine wakes. *J. Wind Eng. Ind. Aerodyn.* **61** 71-85

[9] Smagorinsky J 1963 General Circulation Experiments with de Primitive Equations. Part I: The basic experiment *Mon. Wea. Rev.* **91** 99-164

[10] Lilly D K 1965 On the Computational Stability of Numerical Solutions of Time-Dependent, Nonlinear, Geophysical Fluid Dynamic Problems *Mon. Wea. Rev.* **93** 11-26

[11] Germano M, Piomelli U, Moin P and Cabot W H 1990 A Dynamic Subgrid-Scale Eddy Viscosity Model *Proceedings of Summer Workshop Center of Turbulence Research Stanford University*

[12] Pierce C D and Moin P 2001 Progress-variable approach for Large-Eddy simulation of turbulent combustion *Report No TF-80 Center for Turbulence Research Stanford University*

[13] Wall D, Pierce C D and Moin P 2002 A Semi-implicit Method for Resolution of Acoustic Waves in Low Mach Number Flows *J. Comp. Phys.* **181** 545–563

[14] Larsen G C, Madsen H A and Sørensen N N 2003 Mean wake deficit in the near field *Proceedings of European Wind Energy Conference EWEC'2003*

[15] Helmis C G, Papadopoulos K H, Asimakopoulos D N, Papageorgas P G and Soilemes AT 1995 Study of the near wake structure of a wind turbine comparing measurements from laboratory and full-scale experiments *Solar Energy* **54 (6)** 413-428

[16] Senocak I, Ackerman A S, Kirkpatrik M P, Stevens D E and Mansour N N 2004 Study of near-surface models in large-eddy simulations of neutrally stratified atmospheric boundary layer. *Annual Research Briefs 2004 Center for Turbulence Research Stanford University*

[17] Moeng C H 1984 A large-eddy simulation model for the study of planetary boundary-layer turbulence *J. Atm. Sci.* **41** 2052-2062

[18] Piomelli U and Balaras E 2002 Wall-Layer Models for Large-Eddy Simulations *Annu. Rev. Fluid Mech.* **34** 349-374

[19] Smith D and Taylor G J 1991 Further analysis of turbine wake development and interaction data *Proceedings of the 13th BWEA Wind Energy Conference Swansea UK* 325–331

[20] Talmon A M 1985 The wake of a HAWT model *MT-TNO report 85-010121*

[21] Taylor G J 1987 Fluctuating loads on a wind turbine operating in a wake *Proceedings 9th BWEA Wind Energy Conference Edinburgh* 55–62

[22] Hassan U, Taylor G J and Garrad A D 1988 The dynamic response of wind turbines operating in a wake flow *J. Wind Eng. Ind. Aerodyn.* **27** 113–126

[23] Högström U, Asimakopoulos D N, Kambezidis H, Helmis C G and Smedman A 1988 A Field study of the wake behind a 2 MW wind turbine *Atmos. Env.* **22** 803-820

[24] Højstrup J 1990 Wake measurements on the Nibe wind-turbines in Denmark, Appendix 1. Nibe wake 2: data report-power spectra *Final Report on CEC contract No EN3W.0039.UK(H1)*

[25] Frandsen S 2002 Turbulence and turbulence-generated fatigue loading in wind turbine clusters *Risø-R-1188(EN) Risø National Laboratory Denmark*

[26] Quarton D C 1989 Characterization of wind turbine wake turbulence and its implications on wind farm spacing *Final Report ETSU WN 5096 Department of Energy of the UK Garrad-Hassan Contract*
[27] International Standard IEC 61400-1 Ed.3 2005
[28] Mann J 1998 Wind field simulation *Prob. Engng. Mech.* **13 (4)** 269-282.
[29] Larsen G C and Hansen K S 2003 Spatial coherence of the longitudinal turbulence components *Proceedings of European Wind Energy Conference EWEC'2003*

Acknowledgments
We would like to express our gratitude to Prof. P. Moin and to Prof. J. Alonso (Center for Turbulence Research, Stanford University, California, USA) for their help and advices. Also we are grateful to Spanish Ministry of Science and Education for their financial support in the research project with reference number CGL2005-06966-C07-03 / CLI, and the scholarship of Ángel Jiménez, in the FPU research support program.